Nanoscale fluctuations and surface tension measurements in droplets using phase-resolved low-coherence interferometry

Ru Wang,[1] Taewoo Kim,[2] Mustafa Mir,[2] and Gabriel Popescu[2,*]

[1]Quantitative Light Imaging Laboratory, Department of Mechanical Science and Engineering, Beckman Institute for Advanced Science and Technology, University of Illinois at Urbana-Champaign, Urbana, Illinois 61801, USA

[2]Quantitative Light Imaging Laboratory, Department of Electrical and Computer Engineering, Beckman Institute for Advanced Science and Technology, University of Illinois at Urbana-Champaign, Urbana, Illinois 61801, USA

*Corresponding author: gpopescu@illinois.edu

Received 16 August 2012; revised 15 October 2012; accepted 16 October 2012;
posted 16 October 2012 (Doc. ID 174454); published 13 November 2012

A common-path interferometer was designed with rapidly tunable broadband swept laser source, which provides quantitative phase measurements of nanometer scale motions with very high sensitivity. With this setup, we are able to detect the thermal fluctuations in liquid droplets hanging at the end of an optical fiber. The measured nanoscale displacement fluctuations of various droplet surfaces were used to extract the surface tension. This newly developed technique proved the feasibility of noninvasive, fast, phase-resolved dynamic light scattering measurement of fluid mechanical properties. © 2012 Optical Society of America

OCIS codes: 240.3695, 290.5880, 280.4788.

1. Introduction

Soft materials, such as polymer solutions, colloids, and biological matter, are characterized by multiple characteristic spatiotemporal scales and, as a consequence, their dynamic response to external strains is nontrivial [1]. Microrheology studies the mechanical response of such materials at the microscopic scale. This type of investigation is relevant to a number of fields, especially biology, where cell mechanics is essential for the proper functioning of a living system [2]. It has been shown that optical methods (e.g., dynamic light scattering, fluorescence correlation spectroscopy, optical trapping) are uniquely suitable for studying dynamic properties of soft matter [3]. Recent microrheology techniques rely on applying strain to the fluid through embedded probe particles, either undergoing thermal (Brownian) or externally driven motion [4,5]. In such techniques, the statistics of particle motion is described via the ensemble-averaged mean squared displacements, which requires the recording of multiple trajectories.

Here we present measurements of the nanoscale surface fluctuations associated with small fluid droplets at thermal equilibrium. Using the fluctuation-dissipation theorem [6], these motions are used to infer the mechanical properties of the fluid. Our experimental setup is implemented with optical fibers and relies on phase-resolved interferometry with broadband fields. Amplitude-based low-coherence interferometry (LCI) has been used in the past for performing dynamic light scattering and microrheology measurement [7–11]. However, such amplitude-based techniques are not sensitive enough to detect quantitatively nanometer scale motions;

1559-128X/13/01A177-05$15.00/0

quantitative phase measurements are necessary instead [12,13]. We show that resolving the phase of the field allows us to quantify these fluctuations and extract the respective surface tension coefficient of the liquid.

2. Experimental System

Our experimental system is described in Fig. 1. Light from a swept source, i.e., a laser whose emission wavelength is sweeping a 100 nm spectral range around $\lambda_0 = 1325$ nm at frequency of 8 kHz, is coupled into a single mode fiber coupler. A droplet of interest is in contact with the end of the single-mode optical fiber such that it is suspended in air. The optical field emerging from the fiber core is partially specularly reflected at the fiber/fluid interface, while the transmitted component propagates through the droplet, reflects at the fluid–air interface, and propagates back into the fiber. Thus, the specular field, U_1, can be considered as a reference for the sample field, U_2, which carries information about the position of the droplet surface. The two fields propagate back through the output of the 1×2 fiber coupler and to the detector, which is a conventional OCT balanced detector. The intensity measured by the detector at each optical frequency ω has the form

$$I(\omega) = |U_1(\omega) + U_2(\omega)|^2 = I_1 + I_2 + 2\,\mathrm{Re}[W_{12}(\omega)]. \tag{1}$$

In Eq. (1), $I_{1,2}$ are the intensities of the two fields and W_{12} is the cross-spectral density associated with the two fields, which is defined as [14]

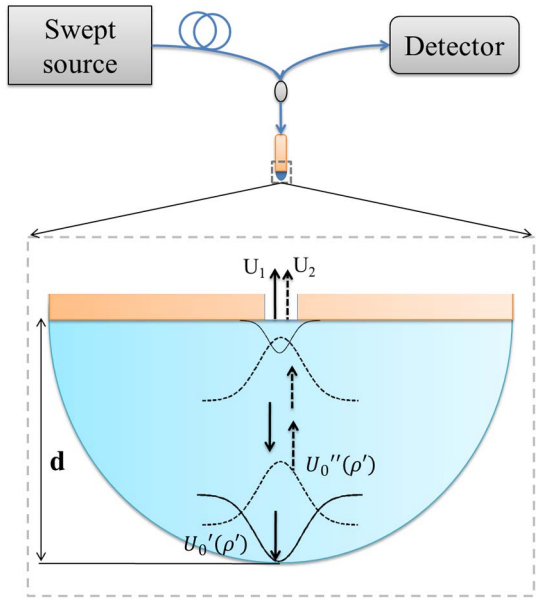

Fig. 1. (Color online) Phase-resolved LCI setup and the expanded view of the fiber tip. The Gaussian field propagation inside the droplet is shown.

$$W_{12}(\omega) = U_1(\omega)U_2{}^*(\omega) = |U_1(\omega)||U_2(\omega)|e^{i(\omega\tau_0+\varphi)}. \tag{2}$$

In Eq. (2), $\tau_0 = 2nd/c$, where n is the refractive index of droplet and d is the thickness of the droplet, for the case of water $n = 1.33$. τ_0 indicates the average time delay associated with U_2 due to propagation through the droplet and φ is the phase shift due to the droplet fluctuations around the average thickness. Note that the two fields are identical in terms of frequency content, except for the phase term and irrelevant scaling of the amplitude. Thus, the modulus of the cross spectral density is the power spectrum of the original field, $S(\omega) = |U_1(\omega)|^2$, and Eq. (2) may be written as

$$W_{12}(\omega) = S(\omega)e^{i(\omega\tau_0+\varphi)}. \tag{3}$$

From Eq. (1), it is clear that experimentally we only have access to the real part of the cross-spectral density. However, the imaginary part of W is obtained using a Hilbert transform as

$$\mathrm{Im}[W_{12}(\omega)] = -\frac{1}{\pi}P\int_{-\infty}^{\infty}\frac{\mathrm{Re}[W_{12}(\omega')]}{\omega-\omega'}\mathrm{d}\omega', \tag{4}$$

where P indicates a principal value integral. From W_{12}, we can now express the cross-correlation function, Γ_{12}, via a Fourier transform

$$\Gamma_{12}(\tau) = \int_{-\infty}^{\infty} W_{12}(\omega)e^{-i\omega\tau}\mathrm{d}\omega. \tag{5}$$

Combining Eqs. (3) and (5), we have

$$\Gamma_{12}(\tau) = \Gamma_0(\tau-\tau_0)e^{i\varphi}, \tag{6}$$

where Γ_0 is the autocorrelation function of either field, the Fourier transform of which is the spectrum, S. Thus, Eq. (6) indicates that the thickness of the droplet can be obtained from this shift as $d = c\tau_0/2n$. The resolution in measuring this thickness is given by the modulus of Γ_0, i.e., the coherence length of the field, which is 17.6 μm in our case. However, the fluctuations of the free surface can be measured with much better accuracy, as this information is carried by the phase of the cross-correlation. Here, it is important to note that, because the two interfering fields are traveling along a common path, the phase relationship between them is extremely stable. The standard deviation of the phase noise was measured by assessing the phase noise in the absence of a sample. The resulting pathlength noise level was measured as 0.62 nm, which sets the limit on the lowest pathlength fluctuation that the instrument can detect. This value translates to a $0.62/(2 \times 1.33) = 0.23$ nm change in thickness associated with the droplet.

3. Principle and Experimental Validation

Our system performs 8,000 scans per second. Figure 2(a) shows an example of time-resolved pathlength distributions obtained by measuring a water droplet. In Fig. 2(b), we show a pathlength profile at approximately $t = 30$ ms, indicated by an arrow in Fig. 2(a). The peak associated with the reflection from the droplet is clearly observed at 656.6 μm. The respective phase measurement is shown in Fig. 2(c). Outside the peak of interest, there are areas where the phase map suffers from phase wrapping due to lack of signal. However, in order to resolve the droplet fluctuations, only the phase information around the reflection peak is necessary. Such time-resolved phase traces are shown in Fig. 2(d) for alcohol, water, and oil droplets. Interestingly, the decay in time of the pathlength signal is due to the evaporation of the droplets. As expected, the alcohol evaporates at the fastest rate, i.e., 8.5 μm/s, and the oil evaporation was measured to be 100 times slower.

To study the droplet fluctuations, we first fit the linear slope and subtract it from the data. The inset of Fig. 2(c) shows the fluctuation track after subtracting the evaporation contribution. The power spectra of these fluctuations for water, alcohol, and oil droplets are shown in Figs. 3(a)–3(c). Interestingly, all the power spectra for these liquids exhibit a power law behavior, with an exponent of $\alpha = -2$. We fit these data with a model borrowed from light scattering by liquid surfaces [15]. For a flat surface of a liquid at thermal equilibrium, the displacement, h has a dependence on the in-plane wavenumber of $k_\perp = \sqrt{k_x^2 + k_y^2}$, and vibrating frequency Ω

$$h(k_\perp, \Omega) = \frac{(1 + i\Omega t_0)^2 - \sqrt{1 + 2i\Omega t_0}}{i\Omega\left[y + (1 + i\Omega t_0)^2 - \sqrt{1 + 2i\Omega t_0}\right]}, \quad (7)$$

where $y = \sigma\rho/4\eta^2 k_\perp$, $t_0 = \rho/2\eta k_\perp^2$, and ρ, η, and σ represent the density, viscosity, and surface tension, respectively. Note that the Gaussian field incident on the droplet surface has its own spatial dependence due to the original field at the end of the fiber and the propagation through the fiber. Thus, the calculation of the field of interest U_2 [Eq. (1)] is performed in several steps. First, the Gaussian field exiting the fiber, $U_0(r) = e^{-r^2/w_0^2}$, (where w_0 is the beam waist and $r = \sqrt{x^2 + y^2}$ is the radial coordinate) propagates through the droplet to yield field $U_0'(\rho')$ at the surface. Upon reflection off the fluctuating surface, the field becomes $U_0''(\rho', \Omega) = U_0'(\rho')e^{i2k_0 h(\rho', \Omega)}$, where k_0 is the light mean wavenumber and ρ' is the conjugate variable to $k_\perp$. After Gaussian propagation back to the fiber, we obtain the final field U_2. Of course, the calculation is performed more efficiently in the $k_\perp$ variable, as in this case the Fresnel propagation of Gaussian beams reduces to a product with a quadratic phase term. The final field U_2 can be expressed symbolically as a function of the initialfield U_0 and displacement distribution h:

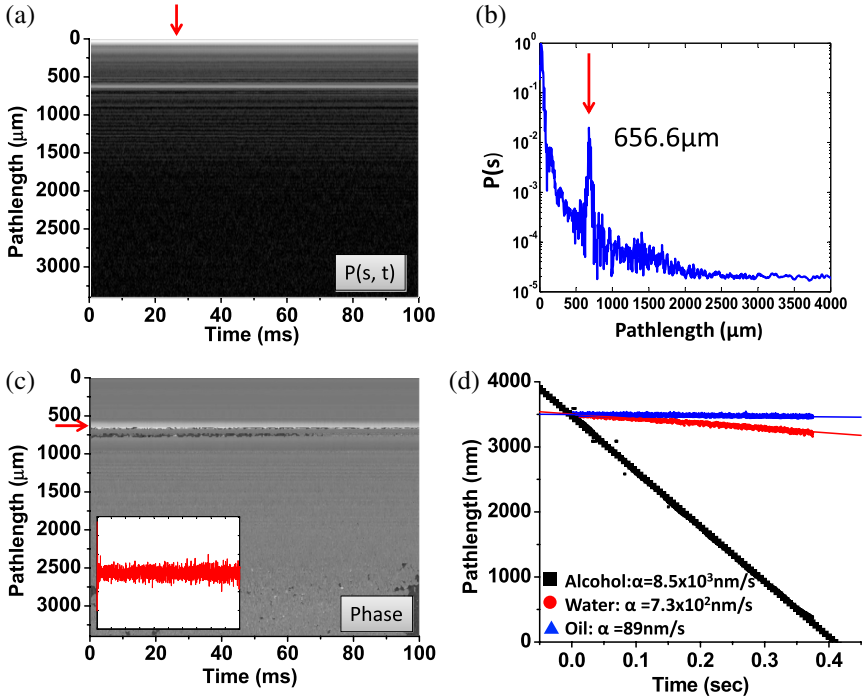

Fig. 2. (Color online) Result of a phase resolved LCI measurement on a liquid droplet. (a) Modulus of the cross-correlation function measured over 100 ms. (b) Vertical profile taken from (a). The arrow indicates the droplet thickness of 656.6 μm. (c) Phase of the cross-correlation function over 100 ms; inset: Horizontal profile at the arrow after removing the slope. (d) Horizontal profile taken from (c) for ethanol, water, and the immersion oil. The evaporation speed calculated from the slope of each profile is shown.

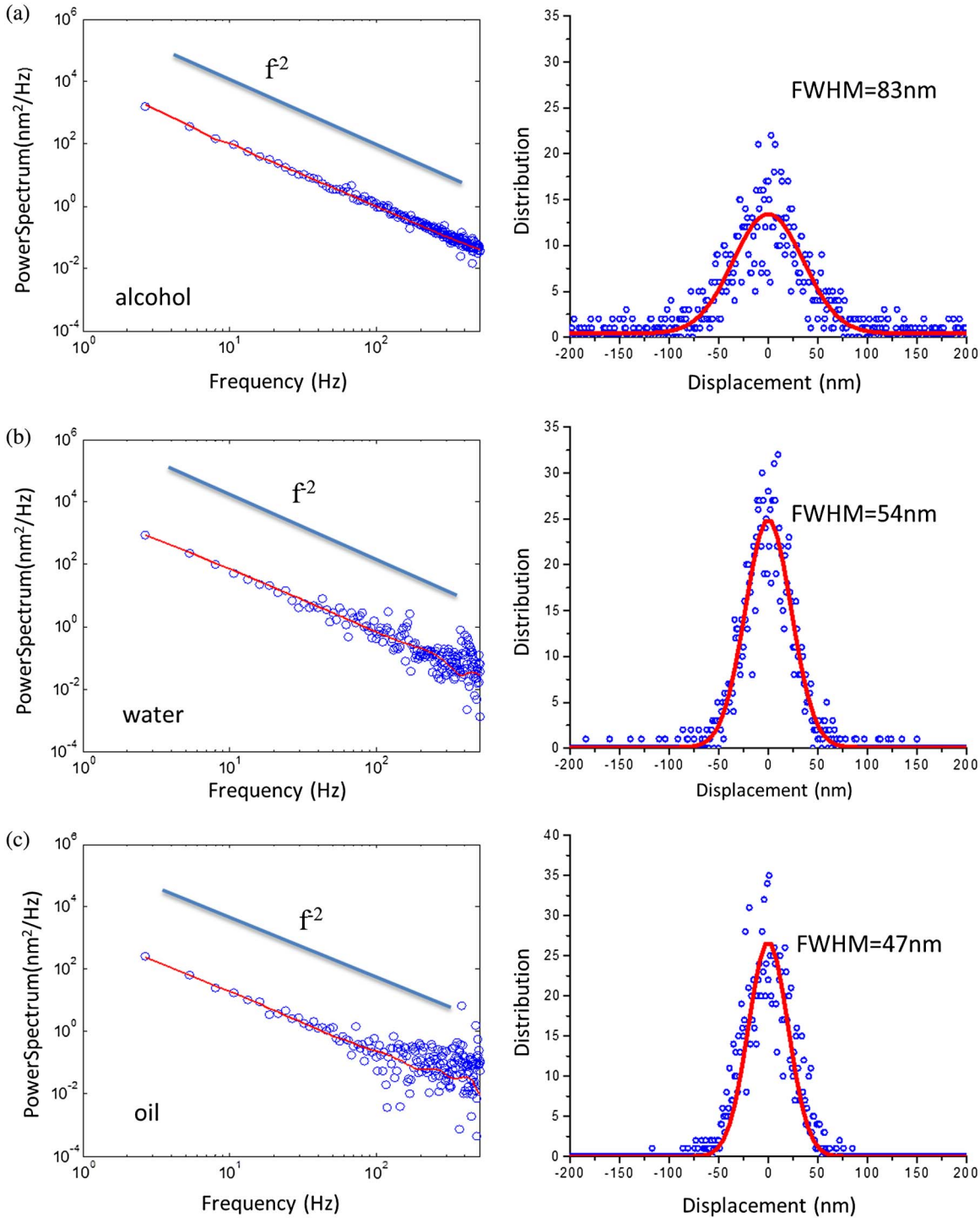

Fig. 3. (Color online) Power spectra of the surface fluctuation (left) and the histogram of the fluctuation amplitude distribution (right) for (a) ethanol, (b) water, and (c) immersion oil. The red lines in the power spectra show the calculated result from our model and the red lines in the histogram plots show Gaussian fits (full width half maxima as indicated).

$$U_2(k_\perp,\Omega) = \exp(i2k_0h(k_\perp,\Omega)^{**} \times \left[U_0(k_\perp)\exp\left(-i\frac{z}{2k_0}k_\perp^2\right)\right]\exp\left(-i\frac{d}{2k_0}k_\perp^2\right). \quad (8)$$

In Eq. (8), symbol ** indicates a 2D convolution integral with respect to variable (K_x, K_y) and d is the thickness of the droplet. Physically, this convolution indicates averaging of the high frequency ripples in the surface (of high $k_\perp$ values). The two products by $\exp(-i(d/2k_0)k_\perp^2)$ indicate Gaussian propagation back and forth through the droplet; plane wave terms, $\exp(ik_0d)$, were ignored as they do not contribute to the fluctuation spectrum. Finally, since the optical fiber integrates the information spatially,

Table 1. Physical Constants of Different Liquids

	n	ρ (kg/m^3)	η (mNs/m^2)	σ (mN/m)
Ethanol	1.36	789	1.2	22.39
Water	1.33	1000	1.0	72.8
Oil	1.518	1093	0.486	106.7

the field U_2 is integrated with respect to $k_\perp$ from 0 to 10,000 rad/m which corresponds to about 1 μm wavelength. The numbers used for this calculation for each liquid is shown in Table 1. All the physical constants are given at room temperature 25°C and the test oil sample was transparent oil, which is widely used for immersion oil objective to increase the resolution of a microscope.

The fluctuating phase of U_2 is extracted as shown in Eq. (6) and its power spectrum is used to fit the experimental data. As indicated by the high quality fit ($r2 = 0.995$), this theoretical model describes the data very well. From the integral of the power spectrum, which is essentially the variance of the fluctuation, the surface tension of ethanol aqueous solutions in different concentrations is measured. As shown in Fig. 4, the measured data agree with the expected values within the experimental errors [16]. The error bars indicate variability from measurement to measurement ($N = 10$ for each concentration). Our errors are surprisingly high despite the sensitivity of our measurement and their understanding requires further investigation. The major possibility could be that the surface fluctuation of droplet is very small (nm scale), so the environmental air flow around it could greatly change its profile, which might contribute large errors. And the laser may increase the local temperature which might result in some variation of physical constants we used to calculate the expected value.

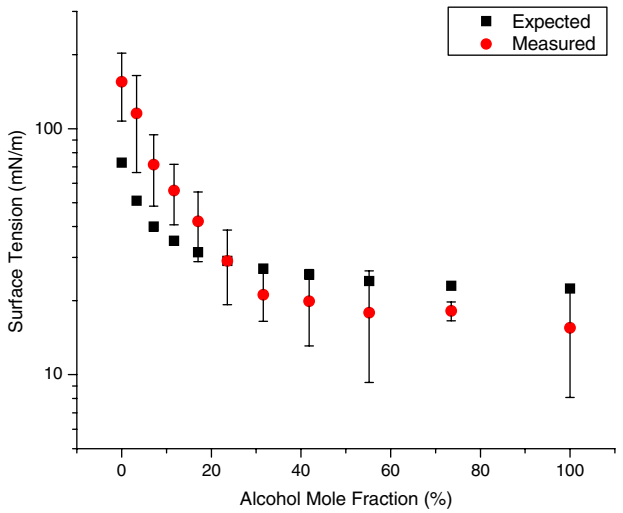

Fig. 4. (Color online) Estimated surface tension of water–ethanol mixture at various mole concentrations (red circles) and expected value of water–ethanol mixture surface tension (black squares). Error bars were obtained from 10 different measurements made for each concentration.

4. Summary and Discussion

In summary, we have introduced a measurement method for nanoscale surface thermal fluctuations of liquid droplets using phase-resolved low coherence interferometry. With the aid of low coherence fields, common-path interferometry, and a fast sampling rate, the sensitivity to thickness fluctuations is a fraction of a nanometer. The data is modeled based on the fluctuations-dissipation theorem to yield the surface tension of liquid droplets. The measurement of ethanol aqueous solutions at different concentrations shows good agreement with the expected physical values. We anticipate that such a fiber optic sensor will find important applications in studying the mechanical properties of small quantities of fluids, e.g., cytoskeleton solutions or blood plasma, without the need for probing beads.

This research was supported by National Science Foundation (CBET 08-46660 CAREER, CBET-1040462 MRI). More information can be found at http://light.ece.illinois.edu/.

References

1. P. M. Chaikin and T. C. Lubensky, *Principles of Condensed Matter Physics* (Cambridge University, 1995).
2. D. H. Boal, *Mechanics of the Cell* (Cambridge University, 2002).
3. R. Borsali and R. Pecora, *Soft-Matter Characterization*, 1st ed. (Springer, 2008).
4. A. J. Levine and T. C. Lubensky, "One- and two-particle microrheology," Phys. Rev. Lett. **85**, 1774–1777 (2000).
5. X. Trepat, L. H. Deng, S. S. An, D. Navajas, D. J. Tschumperlin, W. T. Gerthoffer, J. P. Butler, and J. J. Fredberg, "Universal physical responses to stretch in the living cell," Nature **447**, 592–595 (2007).
6. R. Kubo, "The fluctuation-dissipation theorem," Rep. Prog. Phys. **29**, 255–284 (1966).
7. G. Popescu, A. Dogariu, and R. Rajagopalan, "Spatially resolved microrheology using localized coherence volumes," Phys. Rev. E **65**, 041504 (2002).
8. G. Popescu and A. Dogariu, "Dynamic light scattering in localized coherence volumes," Opt. Lett. **26**, 551–553 (2001).
9. K. K. Bizheva, A. M. Siegel, and D. A. Boas, "Path-length-resolved dynamic light scattering in highly scattering random media: the transition to diffusing wave spectroscopy," Phys. Rev. E **58**, 7664–7667 (1998).
10. A. L. Oldenburg, V. Crecea, S. A. Rinne, and S. A. Boppart, "Phase-resolved magnetomotive OCT for imaging nanomolar concentrations of magnetic nanoparticles in tissues," Opt. Express **16**, 11525–11539 (2008).
11. A. Wax, C. H. Yang, R. R. Dasari, and M. S. Feld, "Measurement of angular distributions by use of low-coherence interferometry for light-scattering spectroscopy," Opt. Lett. **26**, 322–324 (2001).
12. G. Popescu, *Quantitative Phase Imaging of Cells and Tissues* (McGraw-Hill, 2011).
13. B. Varghese, V. Rajan, T. G. van Leeuwen, and W. Steenbergen, "Quantification of optical Doppler broadening and optical path lengths of multiply scattered light by phase modulated low coherence interferometry," Opt. Express **15**, 9157–9165 (2007).
14. L. Mandel and E. Wolf, *Optical Coherence and Quantum Optics* (Cambridge University, 1995).
15. D. Langevin, *Light Scattering by Liquid Surfaces and Complementary Techniques* (Marcel Dekker, 1992).
16. M. Aratono, T. Toyomasu, M. Villeneuve, Y. Uchizono, T. Takiue, K. Motomura, and N. Ikeda, "Thermodynamic study on the surface formation of the mixture of water and ethanol," J. Colloid Interface Sci. **191**, 146–153 (1997).